JOC The Journal of Organic Chemistry

Article

pubs.acs.org/joc

Supramolecular Approach to Enantioselective DNA Recognition Using Enantiomerically Resolved Cationic 4-Amino-1,8-naphthalimide-Based Tröger's Bases

Swagata Banerjee,[†] Sandra A. Bright,[‡] Jayden A. Smith,[†] Jeremy Burgeat,[†] Miguel Martinez-Calvo,[†] D. Clive Williams,[‡] John M. Kelly,*[,†] and Thorfinnur Gunnlaugsson*[,†]

[†]School of Chemistry and Trinity Biomedical Sciences Institute, University of Dublin, Trinity College Dublin, Dublin 2, Ireland

[‡]School of Biochemistry and Immunology and Trinity Biomedical Sciences Institute, Trinity College, Dublin 2, Ireland

Supporting Information

ABSTRACT: The synthesis and photophysical studies of two cationic Tröger's base (TB)-derived bis-naphthalimides **1** and **2** and the TB derivative **6**, characterized by X-ray crystallography, are presented. The enantiomers of **1** and **2** are separated by cation-exchange chromatography on Sephadex C25 using sodium (−)-dibenzoyl-L-tartarate as the chiral mobile phase. The binding of enantiomers with salmon testes (st)-DNA and synthetic polynucleotides are studied by a variety of spectroscopic methods including UV/vis absorbance, circular dichroism, linear dichroism, and ethidium bromide displacement assays, which demonstrated binding of these compounds to the DNA grooves with very high affinity ($K \sim 10^6$ M^{-1}) and preferential binding of (−)-enantiomer. In all cases, binding to DNA resulted in a significant stabilization of the double-helical structure of DNA against thermal denaturation. Compound (±)-**2** and its enantiomers possessed significantly higher binding affinity for double-stranded DNA compared to **1**, possibly due to the presence of the methyl group, which allows favorable hydrophobic and van der Waals interactions with DNA. The TB derivatives exhibited marked preference for AT rich sequences, where the binding affinities follow the order (−)-enantiomer > (±) > (+)-enantiomer. The compounds exhibited significant photocleavage of plasmid DNA upon visible light irradiation and are rapidly internalized into malignant cell lines.

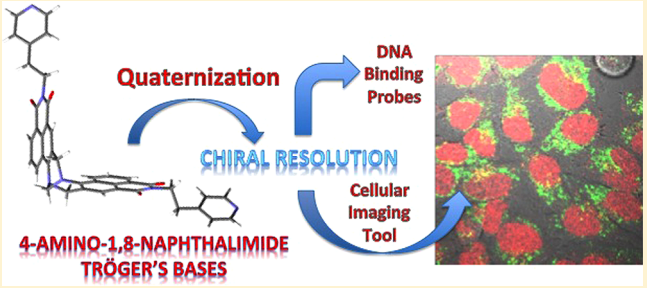

INTRODUCTION

Supramolecular chemistry has become an important tool in the development of targeting structures for use in recognition, sensing, and imaging of biomolecules and as novel therapeutics. Examples of this class of compound employed in such studies are the Tröger's bases (TB), based on a methano-1,5-diazocine ring, which are cleftlike in structure[1] and commonly formed by reacting an aromatic amine with formaldehyde (or formaldehyde equivalent) in the presence of an acid.[2] The TB structures are usually formed as racemic mixtures, but the TB is chiral with a C_2 axis of symmetry due to the presence of two stereogenic nitrogen centers.[2a] In supramolecular chemistry, TB structures have been designed as molecular torsion balances,[3] water-soluble cyclophanes,[2a,b,4] receptors for cations[5a,b] and anions,[5c] dicarboxylic acids,[6] metal-mediated self-assembly systems,[7] molecular tweezers,[8a,b] and optoelectronic devices.[8c] Most of these supramolecules have exploited the "V"-shaped geometry of the TB and have been employed as racemates. Studies with enantiomerically pure TB analogues are relatively limited largely because of the poor availability of the pure enantiomers.[9] In acidic medium, structurally simple TB derivatives have also been reported to undergo racemization through the formation of an iminium intermediate, which greatly hinders their application.[10] In recent times, enantiomeric separation of several TB derivatives has been achieved through diastereomeric salt formation using di-*p*-toluoyltartaric acid[11] or dibenzoyl-L-tartaric acid.[12] With the advent of chiral stationary phases (CSPs), high-performance liquid chromatography using CSPs also appears to be an attractive method for enantiomeric resolution.[13] However, surprisingly, only a few examples of enantiomerically pure TBs have been reported to date.

The development of structures that can enantioselectively recognize and target DNA is of great current interest, particularly in supramolecular chemistry, and the TB building motif offers a great opportunity to achieve that due to its unique structure. The introduction of the TB moiety into organic structures can result in a helical structure, or a twist, which can be similar or opposite to the helicity of double-stranded DNA and may therefore result in enantioselective binding. To this end, Yashima et al.[14] have shown that bis-phenanthroline TB derivatives can indeed induce alteration in the secondary structure of DNA compared to the parent 1,10-

Received: July 28, 2014
Published: September 2, 2014

   dx.doi.org/10.1021/jo501711g | J. Org. Chem. 2014, 79, 9272−9283

phenanthroline, while Demeunynck and co-workers showed selective DNA binding using bis-acridine-based TB structures.[12a,15a] Further studies from the Demeunynck group using a proflavine-phenanthroline TB derivative also showed that the proflavine moiety can intercalate selectively into DNA, while the phenanthroline unit was found to be a minor groove binder.[15b] Bhattacharya and co-workers have also recently demonstrated high cytotoxicity and selective binding of bis-benzimidazole-based TB derivatives to guanine quadruplex DNA derived from a human telomeric sequence.[16] Chiral bis-phenanthroline TB analogues have also been incorporated in the design of Ru(II) complexes targeted to B-DNA,[17] but to the best of our knowledge, no other enantiomerically pure TB structures have been developed to date as DNA targeting structures. With this in mind, we set out to develop such examples based on functional luminescent organic structures.

Amino-1,8-naphthalimides belong to an important family of DNA binding agents that can display antitumor activities both in vitro and in vivo.[18] Several 3- and 4-amino-1,8-naphthalimide-based DNA targeting and cellular imaging agents have been developed by our research group, and we have also explored their application in luminescent and colorimetric sensing.[19,20] Recently, we[20,21] have also reported the development of Tröger's bases incorporating the 4-amino-1,8-naphthalimide moiety,[20] and we showed that naphthalimide-conjugated Ru(II) polypyridyl complexes could also be incorporated into such a TB structure.[21] To date, however, our efforts have been focused on the use of racemic mixtures of such TB naphthalimide derivatives. We have shown that through careful design they possess good DNA binding affinity and exhibit high cytotoxicity against malignant cancer cell lines. Hence, the amino-1,8-naphthalimide-based TBs are unique supramolecular structures that provide several advantageous photophysical properties, such as strong absorption and emission in the visible wavelength region, due to their internal charge-transfer (ICT) nature.[22] In this paper, we present the synthesis and the first examples of enantiomeric resolution of two TB naphthalimide derivatives, namely **1** and **2**, Scheme 2, formed from their corresponding 4-amino-1,8-naphthalimide precursors **3** and **4**. These structures possess alkylpyridinium side chains, which facilitate their interaction with the DNA–phosphate backbone and enhance water solubility. The crucial orthogonal-shaped geometry of these TBs was demonstrated by using solid-state X-ray crystallography of compound **6**, Scheme 1, which was initially synthesized as an intermediate for compound **2**. The DNA interactions of **1**, **2**, and their enantiomers were evaluated using salmon testes (*st*)-DNA and synthetic polynucleotides using various spectroscopic methods, and we show that the results demonstrate enantiopreferential recognition of DNA by these TB structures, which were also examined for their ability to photocleave plasmid DNA and for uptake into HeLa cells.

Scheme 1. Attempted Synthesis of 2 from 6 via 5

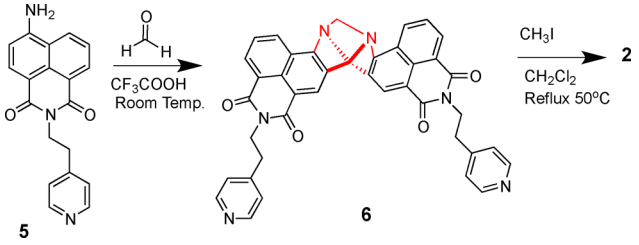

SYNTHESIS AND STRUCTURAL CHARACTERIZATION

The successful syntheses of **1** and **2** are shown in Scheme 2. Both are based on the use of quaternized pyridine units, which

Scheme 2. Synthesis of TB Derivatives 1 and 2 as Racemic Mixtures

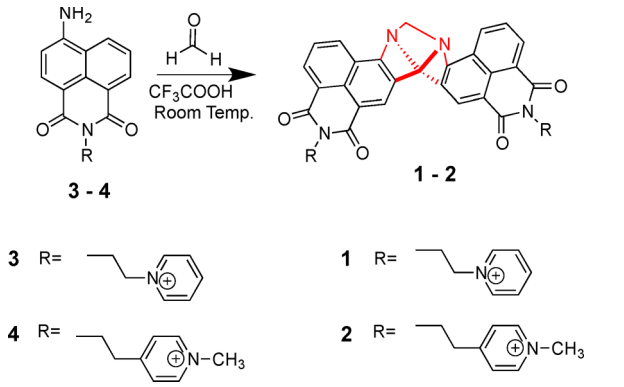

will ensure overall cationic (+2) character for these TB structures and, hence, water solubility, independent of the media pH. The two derivatives only differ in the orientation of their pyridinium moieties relative to the naphthalimide TB structures.[19a,b] Originally, our aim was to make compound **2** by initially forming compound **6**, Scheme 1, and resolve the enantiomers of **6** prior to the quaternization, which was to be achieved by methylation of the pyridine ring of **6** to give **2**. The synthesis of **6** was achieved by reacting compound **5**, also developed in our laboratory,[19b] with paraformaldehyde in neat TFA. During the purification stage, slow evaporation of compound **6** from CH_2Cl_2 solution yielded crystals that were of suitable quality for X-ray crystal structure analysis.

The solid-state structure of compound **6** is shown in Figure 1. This is the first example of a solid-state structural analysis of a naphthalimide-based TB compound. Compound **6** crystallized in a monoclinic system, in the centrosymmetric space group *C*2/*c*. The results clearly show that the methano-1,5-diazocine ring places the two naphthalimide planes almost orthogonal to each other with an angle of 89.17(5)°. The N–CH_2–N bridgehead angle for compound **6** is 111.84°, which is within the range for the same angle in other Troger's base compounds. The molecules pack with pairs of molecules due to the establishment of $\pi\cdots\pi$ stacking interactions between the naphthalimide moieties of two neighboring molecules ($d_{centroid}$ – $d_{centroid}$ 3.553 Å) (see the Supporting Information). Furthermore, CH–π stacking interactions can also be observed in the solid-state packing of **6** between the CH_2 groups of the N–CH_2–N bridgehead and the pyridine group from another neighboring molecule of **6**.

Having successfully synthesized **6**, methylation of the two pyridine units was undertaken using CH_3I. However, while the correct product was formed, judging from crude ^{1}H NMR analysis, it was difficult to purify **2** using standard methods such as column chromatography, as the compound degraded on the column during the purification process, giving naphthalimide byproducts that were difficult to separate from the TB. Consequently, it was necessary to devise a new synthetic

dx.doi.org/10.1021/jo501711g | J. Org. Chem. 2014, 79, 9272–9283

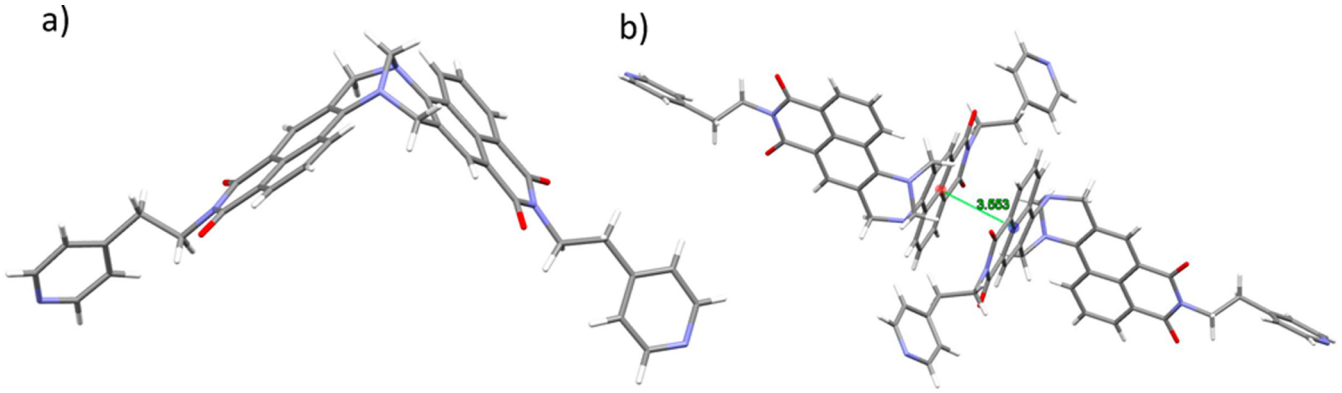

Figure 1. (a) X-ray crystal structure of **6**, showing the orthogonal nature of the two naphthalimide units, forced by the Tröger's base moiety. (b) Packing diagram of **6** when viewed down the crystallographic *b*-axis showing the $\pi\cdots\pi$ interaction which is communicated throughout the network (see packing diagrams when viewed down the crystallographic axes *a*, *b*, and *c* in the Supporting Information).

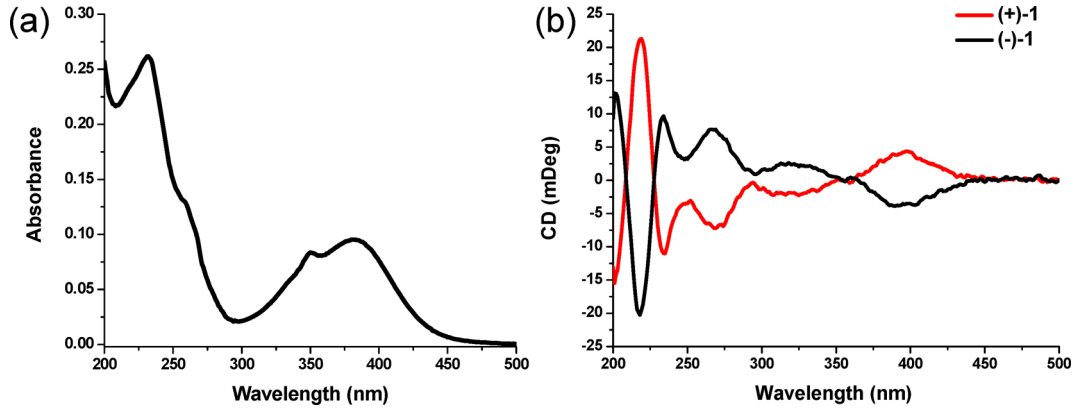

Figure 2. (a) UV/vis absorption and (b) circular dichroism spectra of the (+) and (−) enantiomers of **1** (10 μM) in 10 mM phosphate buffer (pH 7.0).

route for the desired compound **2** which involved using the quaternized pyridinium starting material **4**. Compound **4** had also previously been developed in our laboratory as a DNA binding molecule,[19a,b] and this structure was found to be stable toward acidic conditions, necessary for the formation of **2**. Similarly, precursor **3** was developed for the synthesis of **1**.

Both TB derivatives **1** and **2** were obtained as racemates by reacting, as outlined above, 2 equiv of the precursors **3** or **4** with paraformaldehyde in neat TFA. Upon completion, excess TFA was removed under reduced pressure in the presence of an excess of CH_2Cl_2. The resulting yellow powder was dissolved in CH_3CN and purified on silica gel using a mixture of $CH_3CN/H_2O/NaNO_3$ (saturated) as the eluent. The TB derivatives **1** and **2** were obtained in 57% and 53% yields, respectively. In both cases, the presence of the diazocine ring was confirmed by the appearance of a well-separated doublet of doublets between 4.64 and 5.17 ppm in the ^{1}H NMR (see the Supporting Information, Figures S1−S12), assigned to the methylene protons of the diazocine ring, which also reflect the C_2 symmetry of the molecule.

The full characterization of **1** and **2** is given in the Experimental Section. The photophysical properties of both compounds were investigated in 10 mM phosphate buffer (pH 7.0) solutions. Compound **1** displayed a broad absorption band centered at 382 nm (ε = 12000 M^{-1} cm^{-1}) as shown in Figure 2a. Compound **2** also displayed a similar broad band at 380 nm (ε = 10700 M^{-1} cm^{-1}) (Figure S13a, Supporting Information). For both compounds additional sharp bands at 350 nm and high energy $\pi-\pi^*$ transition bands were observed at lower wavelengths. The full photophysical analysis of these compounds is discussed below.

■ ENANTIOMERIC RESOLUTION OF 1 AND 2

Having successfully made both **1** and **2**, we embarked on the separation of their corresponding enantiomers. The separation of (±)-**1** and (±)-**2** was achieved using a column chromatographic technique developed by Keene and co-workers using Sephadex C25 as the stationary phase and a chiral eluent sodium (−)-dibenzoyl-L-tartarate as the mobile phase.[23] The successful resolution and the enantiomeric purity of (±)-**1** and (±)-**2** were determined by using circular dichroism (CD) spectroscopy.[23]

The CD spectra of the enantiomers of compound **1** in 10 mM phosphate buffer (pH 7) are shown in Figure 2b and those of compound **2** are presented in Figure S13b (Supporting Information). Importantly, enantiomers of both compounds **1** and **2** were found to be stable in 10 mM phosphate buffer (pH 7.0) and did not undergo racemization over a period of 6 months. This is probably due to the mild separation conditions used here (aqueous eluent solution at pH 7.0), which does not promote protonation on the bridgehead nitrogen atoms and induce racemization, since TB derivatives are prone to undergo racemization under acidic condition. The absolute configurations of the enantiomers were tentatively assigned by comparison with the proflavin-derived TB of known configuration, where the (+)-enantiomer was assigned to the (*S*,*S*)

dx.doi.org/10.1021/jo501711g | J. Org. Chem. 2014, 79, 9272−9283

configuration.[12a] However, this should be done with caution as the magnitude and sign of the Cotton effect may change depending on the substituent present on the aromatic ring. These are the first examples of enatiomerically pure 1,8-naphthlimide-based TB derivatives to be isolated by resolution to date.

PHOTOPHYSICAL PROPERTIES

The photophysical properties of the 4-amino-1,8-naphthalimides depend strongly on the polarity and H-bonding ability of solvents due to the "push−pull" nature of the naphthalimide chromophore, originating from the electronic conjugation between the electron-donating amino substituent at the 4-position and electron-accepting imide functional groups.[22] With increase in solvent polarity, the fluorescence spectra of (±)-**1** and (±)-**2** showed significant red shift in emission and decrease in quantum yield of emission (see Figure S14 and Table S1 in the Supporting Information), and both of the compounds were nearly nonemissive in water. These changes are characteristic of an ICT excited state, and similar trends have been also reported by Deprez et al.[24] and Veale et al.[20] for related 4-amino-1,8-naphthalimide-based TB derivatives. Yuan et al. have explained the very weak emission of TB derivatives in aqueous solution in terms of various nonradiative processes such as intramolecular vibrations, enantiomerization, etc.[25] Having investigated the photophysical properties of these TB structures in various solvent systems, we next evaluated their ability to recognize and bind to DNA using both ground- and excited-state spectroscopy.

DNA BINDING INTERACTIONS

UV/vis Absorption Studies. In the presence of st-DNA the UV/vis absorption spectra of the TB derivatives (±)-**1** and (±)-**2** showed significant changes. The UV/vis absorption spectra for (±)-**1** in the presence of increasing concentrations of st-DNA are presented in Figure 3. The addition of st-DNA to a solution of (±)-**1** in 10 mM phosphate buffer (pH 7.0) resulted in a significant hypochromism (35%) of the absorption band centered at 382 nm accompanied by a ca. 10 nm red shift in the λ_{max} (Table 1). An isosbestic point was observed at 412 nm for all DNA/ligand (P/D ratio) concentrations suggesting the presence of two distinct species, i.e., free and bound ligand.

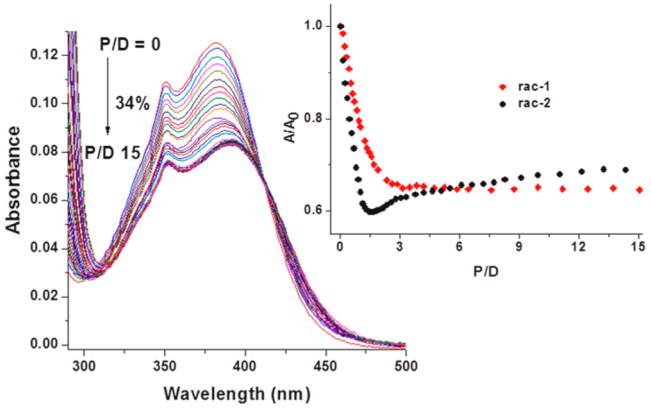

Figure 3. Changes in the UV/vis absorption spectra of (±)-**1** (10.4 μM) in the presence of increasing concentration of st-DNA (0−146 μM) in 10 mM phosphate buffer (pH 7.0). Inset: Plot of relative changes absorbance (A/A_0) vs [DNA base]/[ligand], i.e., P/D for (±)-**1** (at 382 nm) and (±)-**2** (at 380 nm).

Table 1. Summary of Binding Parameters Obtained from the UV/vis Titration of (±)-1, (+)-1, and (−)-1 with st-DNA in 10 mM Phosphate Buffer (pH 7.0)

	(±)-**1**	(+)-**1**	(−)-**1**
λ_{max} (free) (nm)	382	382	382
λ_{max} (bound) (nm)	392	390	392
$\Delta\lambda_{max}$ (nm)	10	8	10
% hypochromism	35	34	36
isosbestic point (nm)	412	418	410
bound P/D	2.5 → 15	2.5 → 15	2.5 → 15
K ($\times 10^6$ M^{-1})[a]	1.17 ± 0.10	1.04 ± 0.14	1.29 ± 0.21
n (bp)	0.32 ± 0.01	0.25 ± 0.01	0.60 ± 0.01

[a]Binding constant determined using the Bard model.

In the case of (±)-**2**, with increasing concentrations of st-DNA, absorbance of the ICT absorption band centered at 380 nm initially decreased by ca. 40% up to P/D of 2 accompanied by a 10 nm bathochromic shift in the λ_{max}. However, with further increase in DNA concentrations (P/D 2−15), the absorbance of this band increased by ca. 15% without any further shift in the λ_{max} (Figure 4 inset and Figure S15, Supporting Information). In 10 mM phosphate buffer (pH 7.0), both the enantiomers of (±)-**1** and (±)-**2** were found to bind strongly to DNA and exhibited spectroscopic changes similar to those observed for the racemic compounds (see the Supporting Information, Figures S16 and S17 and Table S3).

The interactions of (±)-**1**, (±)-**2**, and their enantiomers with st-DNA were also investigated at higher ionic strength in the presence of 50 and 150 mM NaCl. At higher ionic strengths, the overall changes in the absorption spectrum of (±)-**1** were similar to those recorded at low ionic strength; however, the extent of hypochromism was ca. 35% in the presence of 50 mM NaCl (see the Supporting Information, Figure S18a and Table S4) and 29% in the presence of 150 mM NaCl, respectively (see the Supporting Information, Figure S18b and Table S5), with the changes in absorbance plateauing at higher P/D ratios (P/D = 10 → 30 in 50 mM NaCl and P/D = 35 → 100 in 150 mM NaCl, respectively).

At higher ionic strength, the degree of hypochromism observed for the enantiomers of **1** differed significantly. In the presence of 50 mM NaCl, the hypochromism for the 382 nm absorption band was found to be greater for the (−)-**1** enantiomer (38%) compared to the (+)-**1** enantiomer (31%) upon addition of st-DNA with the changes leveling at P/D = 7 for (−)-**1** and P/D = 12 for (+)-**1**, respectively (see the Supporting Information, Figure S18c). The enantiomeric preference was more pronounced at 150 mM NaCl concentration, where the binding constant of (−)-**1** was found to be about three times higher than that of (+)-enantiomer (Figure 4a and Table 2). This behavior was also observed in the reverse salt titration of the two enantiomers, where the fraction of (−)-**1** remained bound at physiological concentration of Na^+ (ca. 150 mM) was higher than that of (+)-**1** (see Figure 4c,d).

Interactions of (+)- and (−)-**2** with st-DNA were also investigated in a similar manner in the presence of 50 and 150 mM NaCl, respectively (see Figure S19, Supporting Information). At higher ionic strengths, the changes observed in the UV/vis absorption spectra of both enantiomers were similar to that of (±)-**2**. However, in the presence of st-DNA, the enantiomers exhibited a significantly different extent of hypochromism and bathochromic shifts under these conditions.

dx.doi.org/10.1021/jo501711g | J. Org. Chem. 2014, 79, 9272−9283

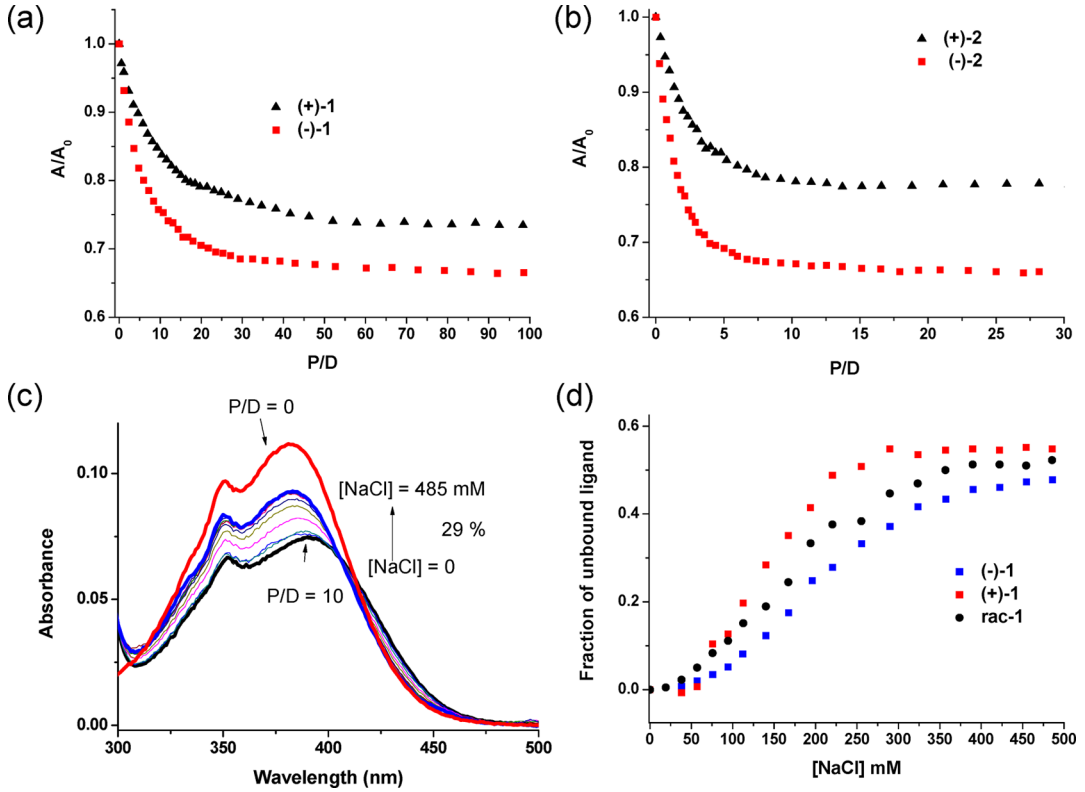

Figure 4. Plot of the changes in the UV/vis absorption spectra of (+)-enantiomer (▲) and (−)-enantiomer (■) of (a) compound **1** and (b) compound **2** in the presence of st-DNA in 10 mM phosphate buffer containing 150 mM NaCl; (c) UV/vis absorption spectra of (±)-**1** (9.3 μM) bound to st-DNA (P/D = 10) in 10 mM phosphate buffer (pH 7.0) upon increasing concentrations of NaCl (0–485 mM); (d) fraction of the ligand liberated with increasing concentrations of NaCl.

Table 2. Binding Constants Determined from the Changes in the UV/vis Absorption Spectra of (±)-1, (±)-2, and Their Enantiomers in 10 mM Phosphate Buffer Containing 0, 50, and 150 mM NaCl

K ($\times 10^6$ M^{-1})[a]	(±)-**1**	(+)-**1**	(−)-**1**	(±)-**2**[b]	(+)-**2**[b]	(−)-**2**[b]
0 mM NaCl	1.17 ± 0.10	1.04 ± 0.14	1.29 ± 0.21	5.31 ± 0.80	5.16 ± 0.68	5.50 ± 0.60
50 mM NaCl	0.73 ± 0.02	0.60 ± 0.02	1.20 ± 0.10	1.10 ± 0.01	0.81 ± 0.07	1.12 ± 0.09
150 mM NaCl	0.20 ± 0.01	0.07 ± 0.005	0.22 ± 0.05	0.74 ± 0.02	0.54 ± 0.05	1.01 ± 0.12

[a]Binding constants determined using the Bard model. [b]P/D ≤ 2 data points were fitted to the Bard model.

In the presence of 50 mM NaCl, changes in absorbance reached a plateau at a P/D = 3 for (−)-**2** and a P/D = 5 for (+)-**2**, respectively (see Figure S19c, Supporting Information). Additionally, the degree of hypochromism at 380 nm was also found to be greater for the (−)-enantiomer (39%) compared to the (+)-enantiomer (35%) upon addition of st-DNA, possibly indicating greater binding affinity of the (−)-**2** toward st-DNA under these conditions. These changes are summarized in Table S6 (Supporting Information). A similar trend was also observed in the presence of 150 mM NaCl, where a greater extent of hypochromism was observed for (−)-**2** upon addition of st-DNA compared to the (+)-enantiomer (Figure 4b). Moreover, the changes in absorbance were found to reach a plateau at a P/D = 10 for (−)-**2**, whereas for the (+)-enantiomer, the changes leveled off at a P/D = 15. The spectral changes for (±)-**2** and its enantiomers in the presence of st-DNA in 10 mM phosphate buffer containing 150 mM NaCl are summarized in Table S7 (Supporting Information). The binding constants for the association of (±)-**1**, (±)-**2**, and their enantiomers with st-DNA were determined by analyzing the changes in absorbance at 382 and 380 nm, respectively, in the presence of st-DNA using the noncooperative model of (i) Bard[26] and (ii) McGhee and von Hippel.[27] In general, the binding constant analysis suggested that the TB derivatives **1** and **2** have substantially higher affinity (ca. 10^6 M^{-1}) for st-DNA (see Table 2) compared to their 4-amino precursors (ca. 10^5 M^{-1}).[19a,b] The binding constant values obtained for **1** and **2** were found to be significantly higher than several acridine-based antitumor agents.[28] Similar binding affinity has also been reported for other 4-amino-1,8-naphthalimide-based TB derivatives.[20] For both of the compounds, the (−)-enantiomer displayed markedly higher binding affinity toward st-DNA than the (+)-enantiomer (Table 2).

In all cases, the substantially stronger binding observed for (±)-**2** and its enantiomers compared to (±)-**1** presumably results from the presence of the additional methyl group, which favors the binding to DNA due to the hydrophobic effect and which has been previously observed for several other DNA binders such as Cr(III) complex bearing a dimethyl dppz ligand,[29] dimethylpteridine,[30] and 2-amino-1,8-naphthyridine derivatives.[31] Moreover, the presence of methyl groups can also increase the polarizability of (±)-**2** and consequently allows better stacking along DNA due to favorable van der Waals interaction.[32]

dx.doi.org/10.1021/jo501711g | J. Org. Chem. 2014, 79, 9272–9283

Table 3. Binding Constants Determined from the Changes in the UV/vis Absorption Spectra of (±)-1, (±)-2, and Their Enantiomers in the Presence of Homopolymeric Sequences in 10 mM Phosphate Buffer (pH 7.0) Containing 50 mM NaCl

K ($\times 10^6$ M^{-1})[a]	(±)-1	(+)-1	(−)-1	(±)-2	(+)-2	(−)-2
Poly(dA-dT)$_2$	0.97 ± 0.06	0.50 ± 0.01	1.66 ± 0.15	3.06 ± 0.02	1.30 ± 0.02	4.18 ± 0.40
Poly(dG-dC)$_2$	0.38 ± 0.01	0.19 ± 0.02	0.45 ± 0.01	1.05 ± 0.03	0.48 ± 0.02	1.20 ± 0.03

[a]Binding constant detexrmined using the noncooperative model of McGhee and von-Hippel.

In order to investigate possible sequence-selective binding of (±)-**1** and (±)-**2** with DNA, their interactions with homopolymers poly(dA-dT)$_2$ and poly(dG-dC)$_2$ were evaluated in a manner similar to that described for st-DNA in 10 mM phosphate buffer containing 50 mM NaCl. Compounds (±)-**1**, (±)-**2**, and their enantiomers were found to interact strongly with the two polynucleotides as indicated by a marked decrease in absorbance of the ICT absorption band and significant red shift in the λ_{max} (the changes in the UV/vis absorption spectra of (±)-**1**, (±)-**2**, and their enantiomers upon binding to poly(dA-dT)$_2$ and poly(dG-dC)$_2$ are shown in Figure S20−S23, Supporting Information). However, the extent of hypochromism and red shift were found to be different for the two enantiomers. As observed previously with st-DNA, the (−)-enantiomers of both compounds exhibited higher affinities for the polynucleotides revealed by a greater degree of hypochromism in the presence of the polynucleotides with the changes reaching a plateau at a lower P/D than that observed for the (+)-enantiomer (see Figures S20−S23, Supporting Information).

The binding constants of (±)-**1**, (±)-**2**, and their enantiomers for the polynucleotides were estimated from the absorbance changes at the ICT absorption band. These values (Table 3) suggest that both the TB derivatives and their enantiomers display a stronger preference for AT-rich sequences. This is perhaps correlated with the higher negative electrostatic potential of the AT rich minor grooves, which facilitates binding of cationic molecules.[33] Additionally, the minor grooves in the AT rich sequences are narrower than those of GC rich regions, which can possibly allow optimal hydrophobic interactions between the ligand and the grooves and favor binding of these "V"-shaped TB derivatives along the minor groove of DNA.

Ethidium Bromide Displacement Assay. The DNA binding affinity of (±)-**1**, (±)-**2**, and their enantiomers were further investigated using an ethidium bromide (EtBr) displacement assay[34] in 10 mM phosphate buffer containing 50 mM NaCl. Changes in the emission spectra of EtBr bound to st-DNA upon titration with (±)-**1** are shown in Figure 5 (see the Supporting Information, Figure S24, for compound (±)-**2**).

In general, additions of (±)-**1**, (±)-**2**, and their enantiomers resulted in a decrease in the fluorescence of EtBr, demonstrating that these TB derivatives displaced EtBr efficiently. The EC_{50} values (concentration of a ligand required to cause a 50% reduction in the fluorescence intensity of EtBr) and the corresponding apparent binding constants (K_{app}) obtained from the titration of EtBr bound to st-DNA with (±)-**1**, (±)-**2**, and their enantiomers are summarized in Table 4. For comparison, the EC_{50} values determined for the 4-amino-1,8-naphthalimide precursors **3** and **4** are also included in Table 4, which shows that the EC_{50} values are significantly smaller for **1** and **2**, and the derived K_{app} values for **1** and **2** were found to be 1 order of magnitude higher than the values obtained for the corresponding 4-amino-1,8-naphthalimide precursors **3** and **4**. This trend is in agreement with the higher

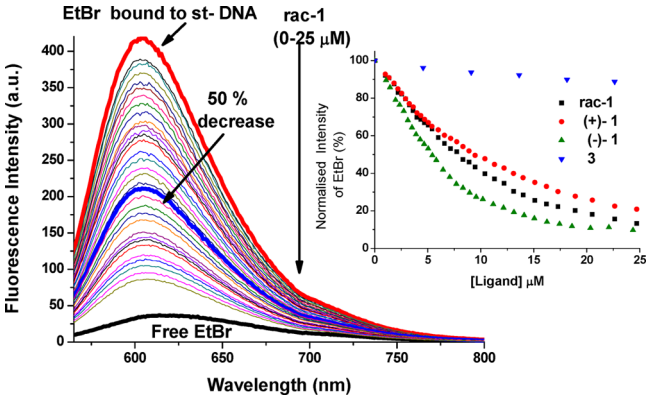

Figure 5. (a) Changes in the emission spectra of EtBr (5 μM) bound to st-DNA, where [EtBr]:[DNA base pair] = 1:2 in the presence of increasing concentrations of (±)-**1** in 10 mM phosphate buffer containing 50 mM NaCl (pH 7.0); (b) normalized fluorescence intensity of EtBr at 605 nm upon addition of (±)-**1** (■), (+)-**1** (●), (−)-**1** (▲), and **3** (▼).

Table 4. EC_{50} Values and K_{app} from the EtBr Displacement Assays in 10 mM Phosphate Buffer Containing 50 mM NaCl (pH 7) ([EtBr] = 5 μM)

compd	EC_{50} (μM)	K_{app} ($\times 10^6$ M^{-1})
(±)-**1**	7.89	0.76
(+)-**1**	9.45	0.63
(−)-**1**	5.50	1.09
(±)-**2**	6.00	1.00
(+)-**2**	6.80	0.88
(−)-**2**	5.10	1.18
3	79.00	0.08
4	90.00	0.06

binding affinity of **1** and **2** determined from the UV/vis titration compared to their precursors **3** and **4** and emphasizes the role of the TB moiety in improving the binding affinity.

Among the TB derivatives, (±)-**2** was found to be more capable of displacing bound EtBr from st-DNA than compound (±)-**1**. This follows the order of their binding affinity for st-DNA as determined from UV/vis absorption titration. Moreover, for both of the TB derivatives the (−)-enantiomer was found to displace EtBr more strongly than the (+)-enantiomer. This is in accordance with the higher binding affinity of the (−)-enantiomer for both of the TB derivatives.

Thermal Denaturation Studies. To further evaluate the DNA binding affinity of the TB derivatives, thermal denaturation of st-DNA was monitored in the presence of (±)-**1**, (±)-**2**, and their enantiomers. The thermal melting curves in the presence of (±)-**1**, (+)-**1**, and (−)-**1** are shown in Figure 6 (and that in the presence of (±)-**2** and its enantiomers in Figure S25, Supporting Information). For comparison, the melting curves for the respective precursors **3** and **4** are also included. In the absence of any ligand, the melting temperature (T_m) value for st-DNA was found to be (68 ± 0.5) °C. In the

dx.doi.org/10.1021/jo501711g | J. Org. Chem. 2014, 79, 9272−9283

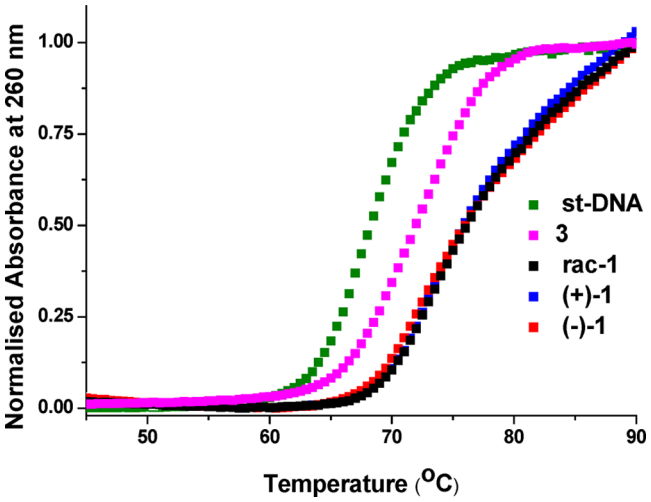

Figure 6. Thermal melting profile of st-DNA (150 μM) in the presence of (±)-**1**, (+)-**1**, (−)-**1** and **3** (P/D 10) in 10 mM phosphate buffer (pH 7.0).

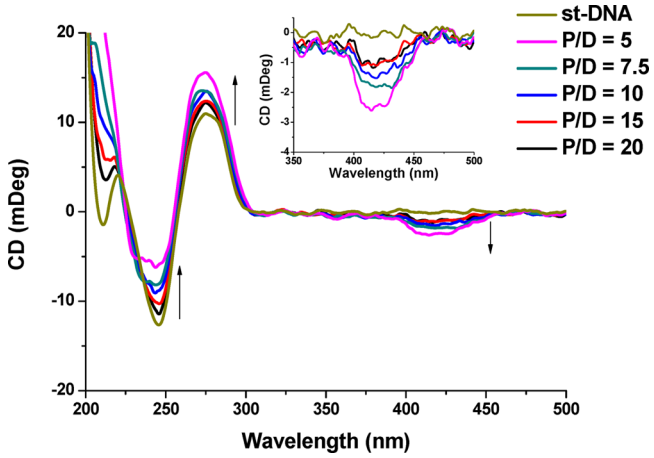

Figure 7. CD spectra of st-DNA (150 μM) in the presence of varying concentrations of (±)-**1** (P/D 0 → 20) in 10 mM phosphate buffer (pH 7.0).

presence of the TB derivatives (±)-**1** and (±)-**2** significant stabilization of the double stranded DNA was observed (ΔT_m > 7 °C). In fact, the denaturation process was found to be still incomplete at 90 °C.

In contrast to these results, only a moderate stabilization was observed for the 4-amino-1,8-naphthalimide precursors **3** and **4** (ΔT_m = 4−5 °C). The high stabilization of DNA in the presence of both TB derivatives correlates with their high binding affinity for st-DNA. Moreover, such a higher extent of stabilization observed for the TB derivatives compared to the 4-amino-1,8-naphthalimide precursors highlights the importance of the rigid "V"-shaped structure of these TB derivatives in stabilizing st-DNA. The thermal denaturation measurements of st-DNA carried out in the presence of the enantiomers of (±)-**1** and (±)-**2** showed that both of the (+)- and (−)-enantiomers stabilized st-DNA to an extent similar to that observed for the racemic mixtures and no significant difference was observed between the enantiomers. This agrees well with the fact that both (+)- and (−)-enantiomers have a comparable high affinity for st-DNA in 10 mM phosphate buffer.

Circular Dichroism Spectroscopy. CD spectroscopy was further used to monitor the changes in DNA conformation upon binding of the TB derivatives.[35] The CD titrations were carried out by monitoring the conformational changes of st-DNA (150 μM) in the presence of increasing concentrations of (±)-**1** and/or (±)-**2**. The CD spectra of st-DNA in the presence of varying concentrations of (±)-**1** are shown in Figure 7. The ellipticity of the negative peak centered at 245 nm increased from −14 to −9.0, while that of the positive peak centered at 275 nm increased from +12 to +16 mdegree. These changes suggest that (±)-**1** interacts strongly with st-DNA as has been observed previously for other naphthalimide-based TB derivatives.[20] More importantly, a weak negative CD signal was observed at ca. 420 nm as the concentration of (±)-**1** was raised. Similar induced CD was also observed in the titration of st-DNA with (±)-**2** (see the Supporting Information, Figure S26a). Analogous behavior has been previously reported for Ru(II) and Cr(III) complexes, where the appearance of such an ICD signal has been explained due to enantiopreferential binding of one of the enantiomers to DNA.[29,36] The weak intensity of the ICD signal observed in this case is presumably due to poor enantioselective binding of (−)-enantiomer in low ionic strength buffer.

Linear Dichroism Spectroscopy. Linear dichroism (LD) spectroscopy was used to investigate the mode of binding of (±)-**1** and (±)-**2** to flow-oriented st-DNA.[35] The LD spectra of st-DNA (400 μM) in the absence and in the presence of (±)-**1** (P/D = 10 →30) are shown in Figure 8, respectively. In the

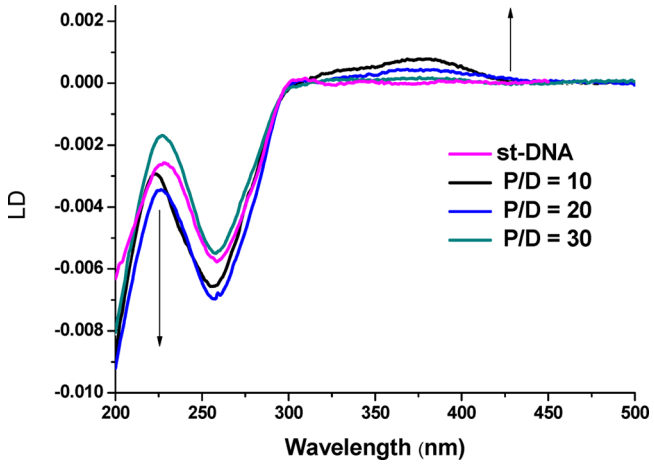

Figure 8. LD spectra of st-DNA (400 μM) in the presence of varying concentrations of (±)-**1** (P/D 0 → 30) in 10 mM phosphate buffer (pH 7.0).

absence of any ligand, a negative LD signal was observed at λ = 260 nm arising from the nearly perpendicular orientation of the transition moments of the DNA bases relative to the DNA helical axis.[35] In the presence of ligand (±)-**1** and/or (±)-**2**, the LD signal for the 260 nm band was still negative; however, a positive LD signal was observed in both cases around 380 nm corresponding to the ICT absorption band of the compounds. Table 5 summarizes the reduced linear dichroism (LD^r) values for the absorption bands at 260 and 380 nm for (±)-**1** and (±)-**2** at P/D ratio of 10, where the ligands should be completely bound to st-DNA. As shown in Table 5, the magnitudes of LD^r value for the DNA absorption region was found to increase slightly in the presence of both (±)-**1** and (±)-**2**, which is consistent with the stiffening of DNA. Additionally the appearance of positive LD signals in the

dx.doi.org/10.1021/jo501711g | J. Org. Chem. 2014, 79, 9272−9283

Table 5. Summary of LDr Data for (±)-1 and (±)-2 in the Presence of st-DNA (error ± 10%)

	LD^r 260 nm	LD^r 380 nm
st-DNA	−0.022	
st-DNA + (±)-**1**	−0.024	+0.026
st-DNA + (±)-**2**	−0.027	+0.021

presence of both (±)-**1** and (±)-**2** suggest that the transition dipoles of these ligands are oriented at angles less than 54.7° relative to the helical axis, indicative of binding of (±)-**1** and (±)-**2** to the DNA groove.

DNA PHOTOCLEAVAGE STUDIES

In order to investigate the photocleavage abilities of the TB derivatives, pBR322 DNA (1 mg/mL) was treated with the TB derivatives and their precursors and irradiated for 60 min with a Hg−Xe lamp filtered to exclude wavelengths less than 360 nm (Figure 9). When they were incubated with (±)-**1** or (±)-**2** (P/D = 10) in the absence of light, significant retardation in the mobility of supercoiled DNA was observed (lanes 3 and 9, respectively). This is perhaps due to the dicationic nature of the TB derivative, binding of which results in reduction in the overall negative charge of plasmid DNA and hence caused reduced mobility. To overcome this, samples containing TB derivatives (±)-**1** and (±)-**2** were extracted with phenol/$CHCl_3$ prior to electrophoresis. The 4-amino precursors **3** and **4** did not induce any significant photocleavage upon photoirradiation, with ca. 18% cleavage being observed (lanes 5 and 11). The failure to observe significant photocleavage activity with the 4-amino analogues is perhaps related to their lower oxidizing potential. In contrast to the 4-amino precursors, the TB derivatives (±)-**1** and (±)-**2** were found to cause significant (85−90%) photocleavage of the plasmid upon irradiation (lanes 6, 7 and lanes 12, 13, respectively), higher than that observed for unsubstituted 1,8-naphthalimide derivative (exhibiting ca. 70% photocleavage, lane 14).[37]

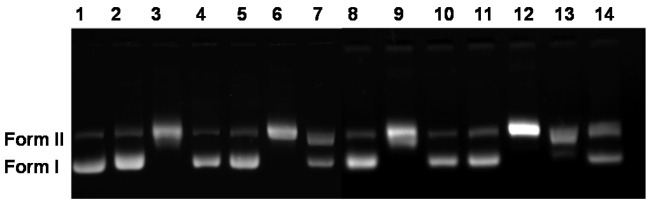

Figure 9. Agarose gel electrophoresis of pBR322 DNA (1 mg/mL) after irradiation at λ > 350 nm in 10 mM phosphate buffer (pH 7.0). Lane: 1, pBR322 control; 2, **3** (P/D 20) nonirradiated; 3, (±)-**1** (P/D 10) nonirradiated; 4, (±)-**1** (P/D 10) nonirradiated + extracted; 5, **3** (P/D 20) irradiated; lane 6, (±)-**1** (P/D 10) irradiated; 7, (±)-**1** (P/D 10) irradiated + extracted; 8, **4** (P/D 20) nonirradiated; 9, (±)-**2** (P/D 10) nonirradiated; 10, (±)-**2** (P/D 10) nonirradiated + extracted; 11, **4** (P/D 20) irradiated; 12, (±)-**2** (P/D 10) irradiated; 13, (±)-2 (P/D 10) irradiated and extracted; 14, reference compound (P/D 20) irradiated.[37]

To verify the possibility of covalent adduct formation between the TB derivatives and DNA upon photoirradiation, a solution of st-DNA containing (±)-**1** at a P/D = 10 was irradiated for 1 h and subjected to the phenol/$CHCl_3$ extraction. UV/vis absorption spectra of the organic layers of both the irradiated and nonirradiated samples showed the presence of the TB derivative (±)-**1** (Supporting Information, Figure S27), suggesting efficient removal of most of the bound ligand from st-DNA. This would not be the case if (±)- **1** was irreversibly bound to DNA.

CELLULAR UPTAKE STUDIES

The cellular uptake and localization studies of (±)-**1** and (±)-**2** in cervical cancer cell lines (HeLa) were carried out using confocal fluorescence microscopy, which demonstrated rapid cellular uptake within 30 min of incubation and apparent localization of the compound within the cytoplasm or at the edge of the nucleus, where the fluorescence presumably arises from the binding of TB derivatives to hydrophobic pockets of proteins or membrane structures (Figure 10).

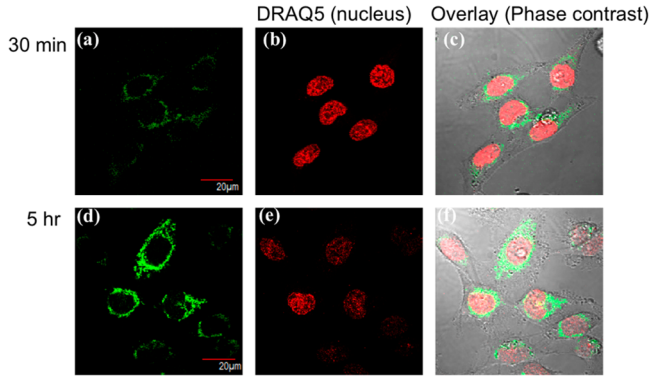

Figure 10. Confocal laser scanning microscopy images of HeLa cells treated with (a) (±)-**1** (20 μM), (b) nuclear stain DRAQ5, (c) overlay of (±)-**1** and DRAQ5 (phase contrast) after 30 min of incubation; (d) (±)-**1** (20 μM), (e) nuclear stain DRAQ5, and (f) overlay of (±)-**1** and DRAQ5 (phase contrast) after 5 h of incubation.

The antiproliferative effects of the compounds were evaluated in HeLa cells using a range of concentrations (1−100 μM) using an Alamar blue viability assay under dark and light irradiated conditions (Supporting Information, Figure S28). These studies suggest that (±)-**1** and (±)-**2** possess significant potential as cellular imaging agents. We are currently investigating the biological effects of these compounds in greater detail.

CONCLUSION

In summary, we have synthesized two novel bis-1,8-naphthalimide-based TB derivatives (±)-**1** and (±)-**2**, which undergo rapid cellular uptake and do not affect cellular viability significantly. We present for the first time a solid-state analysis of the TB naphthalimide structure, which clearly demonstrates the orthogonal nature of the two naphthalimides, forced by the methano-1,5-diazocine ring.

The TB compounds were resolved into their enantiomers by cation-exchange column chromatography using a chiral eluent. The TB derivatives (±)-**1** and (±)-**2** and their enantiomers showed strong affinity for st-DNA (ca. 10^6 M^{-1}) in 10 mM phosphate buffer. The "V"-shaped structure of these TB derivatives presumably exerts steric constraints preventing intercalation of the planar naphthalimide ring. Consequently, the binding site size was found to be significantly less than unity in all cases, suggesting that these molecules bind to the DNA groove and cause significant stiffening of DNA structure. Although our current studies do not provide adequate information regarding the binding of these compounds along

dx.doi.org/10.1021/jo501711g | J. Org. Chem. 2014, 79, 9272−9283

major groove or minor groove, strong preference of (±)-**1** and (±)-**2** and their enantiomers for the AT-rich polynucleotide suggests that these TB derivatives possibly bind to the minor groove of DNA. At low ionic strength buffer, the (+)- and (−)-enantiomers of both **1** and **2** showed comparable DNA binding affinity presumably due to very strong association of the compounds under such conditions. However, at higher ionic strength, the binding affinity of the (−)-enantiomer was found to be greater than that of the (+)-enantiomer for both of the TB derivatives **1** and **2**. This enantioselectivity was more pronounced in the presence of 150 mM NaCl, which closely resembles the physiological Na^+ concentration. This enantioselectivity probably results from the different three-dimensional shape of the enantiomers, which promotes binding of the (−)-enantiomer to the right-handed B-DNA over the (+)-enantiomer. The unique "V"-shaped structure of these TB derivatives combined with their strong affinity for DNA may be used to develop probes for various DNA secondary structures such as "hairpin loop" and "bulged nucleotide sequences", which play important roles during key physiological events like translational initiation, protein cleavage, mutagenesis, etc., and are therefore considered as important drug-targeting sites. We are currently investigating the mode of binding of these TB derivatives, their ability to recognize specific various secondary nucleic acid structures and the consequent biological effects in detail.

EXPERIMENTAL SECTION

General Experimental Details. All chemicals including salmon testes st-DNA, and homopolymeric sequences and solvents were obtained from commercial sources and used without further purification. The DNA concentration per nucleotide was determined spectrophotometrically using the molar extinction coefficients, ε_{260} = 6.6 × 10^3 $M^{-1}cm^{-1}$ for st-DNA, ε_{254} = 8.4 × 10^3 M^{-1} cm^{-1} for poly(dG−dC)$_2$, and ε_{260} = 6.6 × 10^3 M^{-1} cm^{-1} for poly(dA−dT)$_2$, respectively. In titrations the ratio of nucleotide to naphthalimide is given as P/D.

All NMR spectra were recorded using an NMR spectrometer, operating at 400/600 MHz for ^{1}H NMR and 100/150 MHz for ^{13}C NMR, respectively. Chemical shifts were referenced relative to the internal solvent signals. Multiplicities are abbreviated as follows: singlet (s), doublet (d), triplet (t), double triplet (dt). Full assignments of the ^{1}H NMR peaks for the compounds have been confirmed by measuring ^{13}C−^{1}H HSQC and ^{13}C−^{1}H HMBC COSY experiments. Infrared (IR) spectra were recorded on a FT-IR spectrophotometer equipped with an Universal ATR sampling accessory. Mass spectra of the compounds were recorded either on an electrospray mass spectrometer or a MALDI QToF Premier, using HPLC-grade methanol, water, or acetonitrile as carrier solvents. High-resolution mass spectra were obtained by a peak matching method using leucine enkephaline (Tyr-Gly-Gly-Phe-Leu) as the reference (m/z = 556.2771). All accurate masses were quoted to ≤5 ppm. Melting points were determined using a standard digital melting point apparatus.

Solid-State Analysis. X-ray data were collected on a difractometer using graphite-monochromated Mo Kα radiation (λ = 0.71073 Å). Data sets collected on the difractometer were processed using Bruker APEXv2011.8-0 software. The structures were solved by direct methods (SHELXS-97) and refined against all F2 data (SHELXL-97). The hydrogen atom positions were included in the model by electronic density or were geometrically calculated and refined using a riding model, CCDC 1007928.

Enantiomeric Resolution Chromatography. The enantiomers of the TB derivatives were resolved by cation-exchange chromatography on CM Sephadex C25 as the stationary phase and an aqueous solution of (−)-*O*,*O*′-dibenzoyl-L-tartaric acid (as its sodium salt) as the chiral mobile phase (pH 7). The concentration of the eluent was adjusted at 0.05 or 0.07 M to achieve better resolution. In each case, the successful resolution of the enantiomers was achieved after three recycles through a 1 m Perspex column fitted to a peristaltic pump, and in each case, the (−)-enantiomer eluted before the (+)-enantiomer.

UV/vis Absorption Measurements. UV/vis absorption spectra were recorded in quartz cuvettes (10 mm × 10 mm). The wavelength range was 200−800 nm with a scan rate of 600 nm/min. Milli-Q water was used in DNA related work. Phosphate buffer: two 1 M stock solutions of Na_2HPO_4 and NaH_2PO_4 were made up with Milli-Q water. Portions of each solution were diluted together to achieve 10 mM phosphate buffer of pH 7.0, which was then filtered using a 0.45 μM syringe filter. Baseline corrections were performed for all spectral measurements. All solutions were prepared fresh prior to measurement. The UV/vis titrations were carried out by monitoring the changes in the absorption spectra of the ligand of interest in 10 mM phosphate buffer (pH 7.0) upon gradual addition of mononucleotides/st-DNA/polynucleotides. All of the titrations were repeated at least three times to ensure reproducibility.

Fluorescence Measurements. Steady-state fluorescence spectra were recorded using optically dilute solutions (absorbance <0.1) following the same procedure as described for UV/vis titrations. Fluorescence quantum yields of the TB derivatives derivatives were calculated using quinine sulfate in 1 N H_2SO_4 (ϕ_F = 0.546, λ_{ex} = 365 nm) as the reference.[38] For determination of the quantum yields, a number of solutions of the ligand with absorbance ranging from 0.02 to 0.1 were used. Optically matched solutions of the samples and reference were used. The fluorescence emission spectra of the samples and the standard were measured under same experimental settings. The integrated areas under the emission spectra were measured using the in-built software of the spectrofluorimeter. All the quantum yield values reported were within 10% error.

Circular Dichroism and Linear Dichroism. CD spectra were recorded on a spectropolarimeter. Each CD trace represents the average of three scans. Linear dichroism specra were recorded on a CD spectropolarimeter equipped with a linear dichroism accessory. The LD spectra were presented as the average of three scans.

For an oriented sample, linear dichroism is defined as the differential absorption of light polarized parallel (A_{par}) and perpendicular (A_{per}) to a reference axis (eq 1):

$$\mathrm{LD} = A_{par} - A_{per} \tag{1}$$

Quantitative information about the orientation of a chromophore with respect to the reference axis can be obtained from reduced LD (LD^r) as described in eq 2

$$\mathrm{LD}^r = \frac{\mathrm{LD}}{A} = \frac{A_{par} - A_{per}}{A} = \frac{3}{2}S(3\cos^2\alpha - 1) \tag{2}$$

where A is the absorbance of the sample under isotopic condition (i.e., no orientation), S refers to the orientation factor (S = 1 for a perfectly oriented sample, S = 0 for a random orientation), and α is the angle between the transition dipole of the chromophore and the reference axis. The magnitude of S provides information about structural changes in the macromolecule such as lengthening, stiffening, bending etc.

Thermal Denaturation Assays. Thermal denaturation experiments were conducted on an UV/vis spectrophotometer coupled to a Peltier temperature controller. The temperature was ramped from 30 to 90 °C at a rate of 1 °C/min rate, and the absorbance at 260 nm was measured at every 0.2 °C interval. All of the solutions were thoroughly degassed prior to measurement.

DNA Photocleavage Studies. The DNA photocleavage studies were conducted by treating the pBR322 plasmid DNA (1 mg/mL) with the ligand of interest at varying P/D ratios. The samples were then irradiated for 1 h with an Hg−Xe lamp using a green glass filter and water IR filter (λ > 350 nm). An equal volume of the buffer saturated phenol/$CHCl_3$/isoamyl alcohol (25:24:1) mixture was added to the irradiated plasmid DNA samples and mixed gently

dx.doi.org/10.1021/jo501711g | J. Org. Chem. 2014, 79, 9272−9283

using a micropipette. The mixtures were centrifuged for 2 min, and the aqueous layer was carefully removed. The extracted plasmid DNA samples were mixed with a loading dye solution composed of sucrose (40%), xylene−cyanol (0.25%), and bromophenol blue (0.25%) and were then separated using horizontal agarose gel (0.8% w/v) in TBE buffer (8.9 mM Tris-HCl, 8.9 mM boric acid, and 1 mM EDTA, pH 8.0). Electrophoresis was carried out at ca. 5 V/cm (40 mA, 90 V) to separate the covalently closed circular (form **I**), open circular (form **II**), and linear (form **III**) forms of plasmid DNA. The DNA samples were stained using an aqueous solution of ethidium bromide for 90 min, destained with Milli-Q water and visualized using a trans-illuminator equipped with a camera. The ratio of the various DNA forms was estimated using the ImageJ Gel analysis software.

General Biological Procedure. HeLa cells were grown in Dulbecco's Modified Eagle Medium (Glutamax) supplemented with 10% fetal bovine serum and 50 μg/mL penicillin/streptomycin at 37 °C in a humidified atmosphere of 5% CO_2.

Alamar Blue Viability Assay. HeLa cells were seeded at a density of 5×10^3 cells/well in a 96-well plate and treated with the indicated compounds for 48 h. Alamar blue (20 μL) was then added to each well and incubated at 37 °C in the dark for 4 h. Plates were then read on a fluorescent plate reader with excitement and emission wavelengths of 544 and 590 nm, respectively. Experiments were performed in triplicate on three independent days with activity expressed as percentage cell viability compared to vehicle treated controls. All data points (expressed as means ± S.E.M.) were analyzed using GRAPHPAD Prism software.

Confocal Microscopy. HeLa cells were seeded at a density of 1×10^5 cells/well in glass bottom wells and treated with the indicated compounds for up to 48 h. Cells were washed, followed by the addition of fresh media and DRAQ5 (red nuclear stain), followed by viewing using confocal microscopy with a 60× oil immersion lens. Image analysis was performed using FluoView Version 7.1 Software. Compounds were excited by a 405 nm argon laser, emission 480−580 nm, DRAQ5 was excited by a 633 nm red helium−neon laser, emission >650 nm.

*Synthesis of Bis[[2-(N-pyridinium)ethyl]]-9,18-methano-1,8-naphthalimido[b,f][1,5]diazocine (**1**).* Compound **3**·Cl^- (0.303 g, 0.856 mmol) and paraformaldehyde (0.057 g, 1.89 mmol) were stirred in trifluoroacetic acid (TFA) (6 mL) at 20 °C for 12 h under an argon atmosphere. Excess TFA was removed under reduced pressure in the presence of an excess of CH_2Cl_2. The resulting yellow powder was dissolved in CH_3CN and purified on silica gel using a mixture of $CH_3CN/H_2O/NaNO_3$ saturated (88:10:2) as the eluent. The product was precipitated as its PF_6^- salt using ammonium hexafluorophosphate. The PF_6^- salt was dissolved in a minimum amount of MeOH and treated with Amberlite IRA 400 (Cl) ion-exchange resin to convert the product into the chloride form. The product was obtained as a yellow solid after removal of MeOH under reduced pressure in 57% yield (0.18 g): mp dec above 235 °C; HRMS (MALDI) found 707.2169 ([M + Cl]$^+$, $C_{41}H_{32}N_6O_4Cl$ requires 707.2174); δ_H (600 MHz, DMSO-d_6) 9.15 (4H, d, J = 6 Hz, Py-H16, Py-H16′), 8.73 (2H, d, J = 8.4 Hz, Ar-H5, Ar-H5′), 8.57 (2H, t, J = 7.9 Hz, Py-H17, Py-H17′), 8.40 (2H, d, J = 8.0 Hz, Ar-H7, Ar−H7′), 8.05 (4H, t, J = 6.0 Hz, Py-H16, Py-H16′), 8.00 (2H, s, Ar-H2, Ar-H2′), 7.96 (2H, t, J = 8.0 Hz, Ar-H6, Ar-H6′), 5.16 (2H, d, J = 17.5 Hz, Ar-CH_2N), 4.95 and 4.92 (4H, dt, J = 14.0 Hz and J = 7.5 Hz, CH_2, H14, H14′), 4.71 (2H, s, NCH_2N), 4.62 (2H, d, J = 17.5 Hz, Ar-CH_2N), 4.55 (4H, t, J = 7.0 Hz, CH_2, H13, H13′); δ_C (150 MHz), 163.7 (C═O), 163.1 (C═O), 149.3 (C), 145.9 (CH), 145.4 (CH), 130.7 (CH), 130.4 (CH), 129.4 (CH), 127.8 (CH), 127.6 (C), 127.2 (CH), 126.7 (C), 126.1 (C), 122.2 (C), 117.3 (C), 65.9 (CH_2), 59.6 (CH_2), 56.7 (CH_2), 40.7 (CH_2); ν_{max} (neat sample)/cm^{-1} 3374, 1694, 1653, 1595, 1570, 1489, 1459, 1402, 1374, 1354, 1340, 1302, 1258, 1236, 1169, 925, 784.

*Synthesis of Bis[[N-(2-(methylpyridin-1-ium)ethyl)]]-9,18-methano-1,8- naphthalimido[b,f][1,5]diazocine (**2**).* Compound **4**·PF_6^- salt (0.3014 g, 0.631 mmol) and paraformaldehyde (0.054 g, 1.79 mmol) were suspended in TFA and stirred at 20 °C for 12 h under an argon atmosphere. The excess TFA was then removed under reduced pressure in the presence of an excess of DCM. The resulting yellow powder was dissolved in water and purified on silica gel using a mixture of $CH_3CN/H_2O/NaNO_3$ saturated (80:18:2) as the eluent. The product was precipitated as a PF_6^- salt using ammonium hexafluorophosphate. The PF_6^- salt was dissolved in a minimum amount of MeOH and treated with Amberlite IRA 400 (Cl) ion-exchange resin to convert the product into the chloride form. The product was obtained as a yellow solid in 53% yield (0.13 g, 0.168 mmol) after removal of excess MeOH under reduced pressure: mp dec above 175 °C; HRMS (MALDI) found 700.2794 ([M]$^+$, $C_{43}H_{36}N_6O_4$ requires 700.2798); δ_H (600 MHz, CD_3CN), 8.73 (2H, d, J = 8.3 Hz, Ar-H5, Ar-H5′), 8.47 (2H, d, J = 8.0 Hz, Ar-H7, Ar-H7′), 8.46 (4H, d, J = 6.0 Hz, Py-H17, Py-17′), 8.03 (2H, s, Ar-H2, Ar-H2′), 7.90 (4H, d, J = 6 Hz, Py-H16, H16′), 7.89 (2H, t, J = 8.2 Hz, Ar-H6, Ar-H6′), 5.14 (2H, d, J = 17.4 Hz, Ar- CH_2N), 4.67 (2H, s, NCH_2N), 4.63 (2H, d, J = 17.4 Hz, Ar-CH_2N), 4.38 and 4.36 (4H, dt, J = 14.0 Hz and J = 7.0 Hz, CH_2, H13, H13′), 4.23 (6H, s, CH_3), 3.27 (4H, t, J = 7.0 Hz, CH_2, H14, H14′); δ_C (150 MHz) 164.9 (C═O), 164.3 (C═O), 160.9 (C), 150.5 (C), 145.4 (CH), 131.5 (CH), 131.4 (CH), 130.3 (CH), 129.3 (CH), 128.9 (C), 128.3 (C), 128.0 (CH), 127.0 (C), 123.7 (C), 119.2 (C), 67.2 (CH_2), 57.7 (CH_2), 48.6 (CH_3), 40.2 (CH_2), 34.6 (CH_2); ν_{max} (neat sample)/cm^{-1} 3376, 1692, 1647, 1595, 1571, 1459, 1402, 1372, 1339, 1302, 1257, 1231, 1187, 920, 786.

*Synthesis of Bis[[N-(2-(pyridin-4-yl)ethyl)]]-9,18-methano-1,8-naphthalimido[b,f][1,5]diazocine (**5**).* Compound **5** (0.25 g, 0.788 mmol) and paraformaldehyde (0.048 g, 1.59 mmol) were suspended in TFA and stirred at 20 °C for 12 h under an argon atmosphere. The excess TFA was then removed under reduced pressure in the presence of an excess of CH_2Cl_2. The resulting crude product was purified by trituration with methanol resulting in a yellow powder in 60% (0.158 g) yield: mp dec above 252 °C; HRMS (ESI) found 671.2407 ([M + H], $C_{41}H_{31}N_6O_4$ requires 671.2407); δ_H (600 MHz, $CDCl_3$), 8.73 (2H, d, J = 8.5 Hz, Ar-H5, Ar-H5′), 8.62 (2H, d, J = 8.0 Hz, Ar-H7, Ar-H7′), 8.49 (4H, d, J = 6.0 Hz, Py-H17, Py-17′), 8.09 (2H, s, Ar-H2, Ar-H2′), 7.90 (2H, t, J = 8.0 Hz, Ar-H6, H6′), 7.26 (4H, d, J = 6.0 Hz, Py-H16, Py-H16′), 5.18 (2H, d, J = 17.4 Hz, Ar-CH_2N), 4.70 (2H, s, NCH_2N), 4.62 (2H, d, J = 17.4 Hz, Ar-CH_2N), 4.39 (4H, m, CH_2, H13, H13′), 3.02 (4H, t, J = 7.0 Hz, CH_2, H14, H14′); δ_C (150 MHz): 163.8 (C═O), 163.2 (C═O), 149.2 (C), 149.1 (CH), 148.0 (C), 131.0 (CH), 130.5 (CH), 128.9 (CH), 128.2(C), 127.2 (C), 127.1 (CH), 125.2 (C), 124.4 (CH), 122.8 (C), 118.4 (C), 69.9 (CH_2), 57.0 (CH_2), 40.1 (CH_2), 33.4 (CH_2); ν_{max} (neat sample)/cm^{-1} 3058, 2953, 2923, 1689, 1656, 1596, 1570, 1510, 1459, 1440, 1372, 1301, 1255, 1232, 1169, 920, 786.

■ ASSOCIATED CONTENT

Ⓢ Supporting Information

NMR and X-ray characterization, UV/vis, fluorescence, and CD spectroscopy, DNA binding studies using UV/vis titration, CD, LD, EtBr displacement assay, thermal melting, DNA photocleavage, cellular uptake, and viability assay. This material is available free of charge via the Internet at http://pubs.acs.org.

■ AUTHOR INFORMATION

Corresponding Authors

*E-mail: jmkelly@tcd.ie.

*E-mail: gunnlaut@tcd.ie.

Notes

The authors declare no competing financial interest.

■ ACKNOWLEDGMENTS

We thank Science Foundation Ireland (SFI: RFP 2006, RFP 2009, and PI 2010 grants), CSCB, and HEA PRTLI Cycle 4 for financial support. We also thank the Ministerio de Economía y Competitividad of Spain for the funding of a postdoctoral fellowship (to M.M.C.) and thank Trinity College Dublin for a postgraduate studentship (S.B.). We thank Drs. John O'Brien, Manuel Ruether, and Martin Feeney for help with NMR and

mass spectrometry studies. Finally, we thank Dr. Emma B. Veale for her continuous support and help during this work and for introducing the naphthalimide-based Tröger's bases as a research theme into our laboratory. Her massive contribution has and continues to greatly enrich our research endeavors.

REFERENCES

(1) (a) Rúnarsson, Ö. V.; Artacho, J.; Wärnmark, K. *Eur. J. Org. Chem.* **2012**, *2012*, 7015. (b) Dolenský, B.; Havlík, M.; Král, V. *Chem. Soc. Rev.* **2012**, *41*, 3839. (c) Valík, M.; Strongin, R. M.; Král, V. *Supramol. Chem.* **2005**, *17*, 347. (d) Dolenský, B.; Elguero, J.; Král, V.; Pardo, C.; Valík, M. *Adv. Heterocycl. Chem.* **2007**, *93*, 1. (e) Bag, B. G. *Curr. Sci.* **1995**, *68*, 279. (f) Spielman, M. A. *J. Am. Chem. Soc.* **1935**, *57*, 583. (g) Tröger, J. *J. Prakt. Chem.* **1887**, *36*, 225.

(2) (a) Wilcox, C. S. *Tetrahedron Lett.* **1985**, *26*, 5749. (b) Webb, T. H.; Suh, H.; Wilcox, C. S. *J. Am. Chem. Soc.* **1991**, *113*, 8554. (c) Bag, B. G.; Maitra, U. *Synth. Commun.* **1995**, *25*, 1849.

(3) (a) Gardarsson, H.; Schweizer, W. B.; Trapp, N.; Diederich, F. *Chem.—Eur. J.* **2014**, *20*, 4608. (b) Paliwal, S.; Geib, S.; Wilcox, C. S. *J. Am. Chem. Soc.* **1994**, *116*, 4497. (c) Fischer, F. R.; Schweizer, W. B.; Diederich, F. *Angew. Chem., Int. Ed.* **2007**, *46*, 8270. (d) Hof, F.; Scofield, D. M.; Schweizer, W. B.; Diederich, F. *Angew. Chem., Int. Ed.* **2004**, *43*, 5056.

(4) (a) Wilcox, C. S.; Adrian, J. C.; Webb, T. H.; Zawacki, F. J. *J. Am. Chem. Soc.* **1992**, *114*, 10189. (b) Cowart, M. D.; Sucholeiki, I.; Bukownik, R. R.; Wilcox, C. S. *J. Am. Chem. Soc.* **1988**, *110*, 6204.

(5) (a) Manjula, A.; Nagarajan, M. *Tetrahedron* **1997**, *53*, 11859. (b) Kim, K.; Choe, J. I. *Bull. Korean Chem. Soc.* **2006**, *27*, 1737. (c) Boyle, E. M.; Comby, S.; Molloy, J. K.; Gunnlaugsson, T. *J. Org. Chem.* **2013**, *78*, 8312.

(6) (a) Satishkumar, S.; Periasamy, M. *Tetrahedron: Asymmetry* **2009**, *20*, 2257. (b) Kobayashi, T.; Moriwaki, T. *Heterocycles* **2004**, *62*, 399. (c) Goswami, S.; Ghosh, K.; Dasgupta, S. *J. Org. Chem.* **2000**, *65*, 1907.

(7) (a) Hawes, C. S.; Fitchett, C. M.; Batten, S. R.; Kruger, P. E. *Inorg. Chim. Acta* **2012**, *389*, 112. (b) Weilandt, T.; Kiehne, U.; Bunzen, J.; Schnakenburg, G.; Lutzen, A. *Chem.—Eur. J.* **2010**, *16*, 2418. (c) Favera, N. D.; Kiehne, U.; Bunzen, J.; Hytteballe, S.; Lutzen, A.; Piguet, C. *Angew. Chem., Int. Ed.* **2010**, *49*, 125. (d) Weilandt, T.; Kiehne, U.; Schnakenburg, G.; Lutzen, A. *Chem. Commun.* **2009**, 2320. (e) Kiehne, U.; Weilandt, T.; Lutzen, A. *Eur. J. Org. Chem.* **2008**, 2056. (f) Kiehne, U.; Weilandt, T.; Lutzen, A. *Org. Lett.* **2007**, *9*, 1283.

(8) (a) Parchansky, V.; Matejka, P.; Dolensky, B.; Havlik, M.; Bour, P. *J. Mol. Struct.* **2009**, *934*, 117. (b) Havlík, M.; Král, V.; Kaplanek, R.; Dolenský, B. *Org. Lett.* **2008**, *10*, 4767. (c) Yuan, C. X.; Xin, Q. A.; Liu, H. J.; Wang, L.; Jiang, M. H.; Tao, X. T. *Sci. China Chem.* **2011**, *54*, 587.

(9) Recent examples include: (a) Kamiyama, T.; Ozer, M. S.; Otth, E.; Deska, J.; Cvengros, J. *ChemPlusChem.* **2013**, *75*, 1510. (b) Meyer-Eppler, G.; Vogelsang, E.; Benkhauser, C.; Schneider, A.; Schnakenburg, G.; Lutzen, A. *Eur. J. Org. Chem.* **2013**, 4523. (c) Dolenský, B.; Kessler, J.; Jakubek, M.; Havlík, M.; Čejka, J.; Novotná, J.; Král, V. *Tetrahedron Lett.* **2013**, *54*, 308. (d) Benkhauser-Schunk, C.; Wezisla, B.; Urbahn, K.; Kiehne, U.; Daniels, J.; Schnakenburg, G.; Neese, F.; Lutzen, A. *ChemPlusChem* **2012**, *77*, 396.

(10) Greenberg, A.; Molinaro, N.; Lang, M. *J. Org. Chem.* **1984**, *49*, 1127.

(11) (a) Hamada, Y.; Mukai, S. *Tetrahedron: Asymmetry* **1996**, *7*, 2671. (b) Tálas, E.; Margitfalvi, J.; Machytka, D.; Czugler, M. *Tetrahedron: Asymmetry* **1998**, *9*, 4151.

(12) (a) Tatibouet, A.; Demeunynck, M.; Andraud, C.; Collet, A.; Lhomme, J. *Chem. Commun.* **1999**, 161. (b) Satishkumar, S.; Periasamy, M. *Tetrahedron: Asymmetry* **2006**, *17*, 1116.

(13) (a) Ikai, T.; Yamamoto, C.; Kamigaito, M.; Okamoto, Y. *Chirality* **2005**, *17*, 299. (b) Didier, D.; Tylleman, B.; Lambert, N.; Vande Velde, C. M. L.; Blockhuys, F.; Collas, A.; Sergeyev, S. *Tetrahedron* **2008**, *64*, 6252. (c) Kiehne, U.; Bruhn, T.; Schnakenburg, G.; Fröhlich, R.; Bringmann, G.; Lützen, A. *Chem.—Eur. J.* **2008**, *14*, 4246. (d) Sergeyev, S.; Diederich, F. *Angew. Chem., Int. Ed.* **2004**, *43*, 1738.

(14) Yashima, E.; Akashi, M.; Miyauchi, N. *Chem. Lett.* **1991**, 1017.

(15) (a) Bailly, C.; Laine, W.; Demeunynck, M.; Lhomme, J. *Biochem. Biophys. Res. Commun.* **2000**, *273*, 681. (b) Baldeyrou, B.; Tardy, C.; Bailly, C.; Colson, P.; Houssier, C.; Charmantray, F.; Demeunynck, M. *Eur. J. Med. Chem.* **2002**, *37*, 315.

(16) Paul, A.; Maji, B.; Misra, S. K.; Jain, A. K.; Muniyappa, K.; Bhattacharya, S. *J. Med. Chem.* **2012**, *55*, 7460.

(17) (a) Ezadyar, S. A.; Kumbhar, A. S.; Kumbhar, A. A.; Khan, A. *Polyhedron* **2012**, *36*, 45. (b) Claessens, N.; Pierard, F.; Bresson, C.; Moucheron, C.; Kirsch-De Mesmaeker, A. *J. Inorg. Biochem.* **2007**, *101*, 987. (c) Bresson, C.; Luhmer, M.; Demeunynck, M.; Kirsch-De Mesmaeker, A.; Pierard, F. *Tetrahedron Lett.* **2004**, *45*, 2863.

(18) (a) Banerjee, S.; Veale, E. B.; Phelan, C. M.; Murphy, S. A.; Tocci, G. M.; Gillespie, L. J.; Frimannsson, D. O.; Kelly, J. M.; Gunnlaugsson, T. *Chem. Soc. Rev.* **2013**, *42*, 1601. (b) Lee, M. H.; Jeon, H. M.; Han, J. H.; Park, N.; Kang, C.; Sessler, J. L.; Kim, J. S. *J. Am. Chem. Soc.* **2014**, *136*, 8430. (c) Yang, Q.; Yang, P.; Qian, X.; Tong, L. *Bioorg. Med. Chem. Lett.* **2008**, *18*, 6210. (d) Xie, S.-Q.; Zhang, Y.-H.; Li, Q.; Xu, F.-H.; Miao, J.-W.; Zhao, J.; Wang, C.-J. *Apoptosis* **2012**, *17*, 725. (e) Kilpin, K. J.; Clavel, C. M.; Edafe, F.; Dyson, P. J. *Organometallics* **2012**, *31*, 7031. (f) Wu, X.; Sun, X.; Guo, Z.; Tang, J.; Shen, Y.; James, T. D.; Tian, H.; Zhu, W. *J. Am. Chem. Soc.* **2014**, *136*, 3579. (g) Hettiarachchi, S. U.; Prasai, B.; McCarley, R. L. *J. Am. Chem. Soc.* **2014**, *136*, 7575. (h) Silvers, W. C.; Prasai, B.; Burk, D. H.; Brown, M. L.; McCarley, R. L. *J. Am. Chem. Soc.* **2013**, *135*, 309. (i) Lee, M. H.; Kim, J. Y.; Han, J. H.; Bhuniya, S.; Sessler, J. L.; Kang, C.; Kim, J. S. *J. Am. Chem. Soc.* **2013**, *134*, 12668. (j) Braña, M. F.; Cacho, M.; Garcia, M. A.; de Pascual-Teresa, B.; Ramos, A.; Acero, N.; Llinares, F.; Munoz-Mingarro, D.; Abradelo, C.; Rey-Stolle, M. F.; Yuste, M. *J. Med. Chem.* **2002**, *45*, 5813.

(19) Examples of DNA targeting agents include: (a) Banerjee, S.; Kitchen, J. A.; Gunnlaugsson, T.; Kelly, J. M. *Org. Biomol. Chem.* **2013**, *11*, 5642. (b) Banerjee, S.; Kitchen, J. A.; Gunnlaugsson, T.; Kelly, J. M. *Org. Biomol. Chem.* **2012**, *10*, 3033. (c) Ryan, G. J.; Elmes, R. B. P.; Quinn, S. J.; Gunnlaugsson, T. *Supramol. Chem.* **2012**, *24*, 175. (d) Ryan, G. J.; Quinn, S.; Gunnlaugsson, T. *Inorg. Chem.* **2007**, *47*, 401. Examples of luminescent and colorimetric sensors include: (e) Veale, E. B.; Tocci, G. M.; Pfeffer, F. M.; Kruger, P. E.; Gunnlaugsson, T. *Org. Biomol. Chem.* **2009**, *7*, 3447. (f) Duke, R. M.; Gunnlaugsson, T. *Tetrahedron Lett.* **2007**, *48*, 8043. (g) Duke, R. M.; Gunnlaugsson, T. *Tetrahedron Lett.* **2011**, *52*, 1503. (h) Ali, H. D. P.; Kruger, P. E.; Gunnlaugsson, T. *New J. Chem.* **2008**, *32*, 1153. (i) Kitchen, J. A.; Martinho, P. N.; Morgan, G. G.; Gunnlaugsson, T. *Dalton Trans.* **2014**, *43*, 6468.

(20) (a) Veale, E. B.; Frimannsson, D. O.; Lawler, M.; Gunnlaugsson, T. *Org. Lett.* **2009**, *11*, 4040. (b) Veale, E. B.; Gunnlaugsson, T. *J. Org. Chem.* **2010**, *75*, 5513.

(21) Elmes, R. B. P.; Erby, M.; Bright, S. A.; Williams, D. C.; Gunnlaugsson, T. *Chem. Commun.* **2012**, *48*, 2588.

(22) Duke, R. M.; Veale, E. B.; Pfeffer, F. M.; Kruger, P. E.; Gunnlaugsson, T. *Chem. Soc. Rev.* **2010**, *39*, 3936.

(23) (a) Fletcher, N. C.; Keene, F. R. *J. Chem. Soc., Dalton Trans.* **1999**, 683. (b) Fletcher, N. C.; Junk, P. C.; Reitsma, D. A.; Keene, F. R. *J. Chem. Soc., Dalton Trans.* **1998**, 133.

(24) Deprez, N. R.; McNitt, K. A.; Petersen, M. E.; Brown, R. G.; Lewis, D. E. *Tetrahedron Lett.* **2005**, *46*, 2149.

(25) (a) Yuan, C. X.; Tao, X. T.; Wang, L.; Yang, J. X.; Jiang, M. H. *J. Phys. Chem. C* **2009**, *113*, 6809. (b) Yuan, C. X.; Tao, X. T.; Ren, Y.; Li, Y.; Yang, J. X.; Yu, W. T.; Wang, L.; Jiang, M. H. *J. Phys. Chem. C* **2007**, *111*, 12811.

(26) Carter, M. T.; Rodriguez, M.; Bard, A. J. *J. Am. Chem. Soc.* **1989**, *111*, 8901.

(27) McGhee, J. D.; von Hippel, P. H. *J. Mol. Biol.* **1974**, *86*, 469.

(28) (a) Wilson, W. R.; Baguley, B. C.; Wakelin, L. P. G.; Waring, M. *Mol. Pharmacol.* **1981**, *20*, 404. (b) Baguley, B. C.; Denny, W. A.; Atwell, G. J.; Cain, B. F. *J. Med. Chem.* **1981**, *24*, 170.

(29) Vasudevan, S.; Smith, J. A.; Wojdyla, M.; McCabe, T.; Fletcher, N. C.; Quinn, S. J.; Kelly, J. M. *Dalton Trans.* **2010**, *39*, 3990.
(30) Dai, Q.; Xu, C.-Y.; Sato, Y.; Yoshimoto, K.; Nishizawa, S.; Teramae, N. *Anal. Sci.* **2006**, *22*, 201.
(31) Sato, Y.; Nishizawa, S.; Yoshimoto, K.; Seino, T.; Ichihashi, T.; Morita, K.; Teramae, N. *Nucleic Acids Res.* **2009**, *37*, 1411.
(32) (a) Sowers, L. C.; Shaw, B. R.; Sedwick, W. D. *Biochem. Biophys. Res. Commun.* **1987**, *148*, 790. (b) Wang, S.; Kool, E. T. *Biochemistry* **1995**, *34*, 4125.
(33) Fairley, T. A.; Tidwell, R. R.; Donkor, I.; Naiman, N. A.; Ohemeng, K. A.; Lombardy, R. J.; Bentley, J. A.; Cory, M. *J. Med. Chem.* **1993**, *36*, 1746.
(34) Boger, D. L.; Fink, B. E.; Brunette, S. R.; Tse, W. C.; Hedrick, M. P. *J. Am. Chem. Soc.* **2001**, *123*, 5878.
(35) Nordén, B.; Rodger, A.; Dafforn, T. *Linear Dichroism and Circular Dichroism*; The Royal Society of Chemistry: London, 2010.
(36) Hiort, C.; Lincoln, P.; Norden, B. *J. Am. Chem. Soc.* **1993**, *115*, 3448.
(37) Rogers, J. E.; Abraham, B.; Rostkowski, A.; Kelly, L. A. *Photochem. Photobiol.* **2001**, *74*, 521.
(38) Crosby, G. A.; Demas, J. N. *J. Phys. Chem.* **1971**, *75*, 991.
(39) Sheldrick, G. M. *Acta Crystallogr., Sect. A* **2008**, *A64*, 112.